Chalcogenide Letters Vol. 21, No. 4, April 2024, p. 343 - 354

Properties investigation of ZnS/porous silicon heterojunction for gas sensing

F. B. Mohammed Ameen[a], M. H. Younus[b], G. G. Ali[c,*]
Physics Department, College of Education for Pure Science, Mosul University, Iraq

In this work, the gas sensing properties of ZnS/Porous silicon heterostructures have been investigated. . Zinc sulfide(ZnS) with high gas sensing performance is successfully synthesized over the Porous silicon substrate by the spray pyrolysis method. The properties of the as-prepared samples were characterized X-ray diffraction (XRD), scanning electron microscope (SEM), Fourier transform spectrum (FTIR) and optical properties. The results reveal that the properties of the ZnS/Porous silicon heterostructures enhanced when the when the ZnS concentration is increased. The performance ZnS/Porous silicon as a gas-sensing show that the maximum sensitivity is found to be 5.11 at ZnS concentration of 0.5 M and etching time of 15 min compared to the other sensitivities. The ZnS-PSi heterojunction based gas sensor may be used for UV-light photo-detectors due to a valuable properties such as high sensitivity and fast response.

(Received February 11, 2024; Accepted April 26, 2024)

Keywords: ZnS, Porous silicon, SEM, XRD, Gas sensor

1. Introduction

Porous silicon has attracted great attention due to its photoluminescence at room temperature in the visible light range [1, 2]. High efficiency can be obtained using nanoporous silicon with different physical properties compared to its bulk structure, including a wide energy gap and a low reflection coefficient compared to crystalline c-Si [3,4]. Because of this feature, it has been used as sensors for detecting gases, vapors and humidity. Zinc sulfide (ZnS) is an inorganic material with a wide direct energy gap of 3.7eV, which belongs to the halogen elements in the II-VI periodic table. Furthermore, the ZnS have different applications, such as ultraviolet light-emitting diodes (LEDs) [5], light conversion electrodes and efficient phosphors in Flat screens , solar cells [6,7] and in particular its use as gas sensors [8,9].Due to the important applications of thin films, different methods were invented for their deposition, some of these methods are complex and others simple. The choice of the deposition method depends on several factors, the most important of which are the type of materials used, the final specifications of the membrane, the type of substrate and benefit of using the prepared membranes and its production cost [10, 11]. The Spray pyrolysis method is one of the most important techniques for thin film deposition. It is easy to use and inexpensive. This method can be used to obtain high quality thin films by controlling different parameters, such as temperature, dimension between the substrate, the material and the spray rate[12]. The principle of preparing membranes by spraying with pyrolysis involves spraying a solution of the material from which the membrane is to be prepared[13]. They are in the form of very thin droplets on heated substrates at a specific temperature that depends on the type of material used, so that a thermochemical reaction (pyrolysis of solid compounds formed on the surface of the substrate) occurs between the atoms of the material and the hot substrate, and as a result of this reaction a thin film is formed [14, 15]. Based on previous research, depositing a zinc sulfide layer (ZnS) on porous silicon can be enhanced the sensitivity to light, expand the wavelength of light detection, enhance the response speed and sensitivity in gas sensing [16, 17, 18].The aim of this manuscript is to study the structure (XRD) and optical properties (UV-spectrophotometer) as well as gas sensor of ZnS/PSi heterojunction.

* Corresponding author: dr.ghazwan39@uomosul.edu.iq
https://doi.org/10.15251/CL.2024.214.343

2. Experimental method

2.1. Preparation details of porous silicon

Porous silicon substrates were obtained by electrochemical etching of p-type (111) oriented silicon (c-Si) wafers with a resistivity of 1–10 Ω cm. Silicon wafers were cleaned with propanol and alcohol using an ultrasonic bath for 5 min. The c-Si wafers were rinsed with deionized water, dried with N_2 flux, after that the samples immersed in mixed hydrofluoric acid (20%HF) and ethanol (99%). The anodizing cell consists of two cylinders made of Teflon with identical diameters. The upper layer contains a cylindrical cavity designated for the etching solution, while the lower layer is completely solid. The circle metal made of steal-steel is placed on the lower cylinder and the wafer Si is placed on it and filled with an etching solution as the Figure 1a. The etching time was carried out for 5, 10, 15 min and the fixed current density of 12 mA/cm^2.

2.2. Synthesis and deposition of ZnS

ZnS thin films on p-Si substrates were obtained by spray pyrolysis. Zinc chloride ($ZnCl_2$) and sodium sulfide (Na_2S) were Sigma Aldrich, reagent grade, 97% purity. The $ZnCl_2$ and Na_2S were mixed in deionized water solutions at (0.1, 0.3 and 0.5M) as Table 1. The stirrer of acetate solution was for 40 min at room temperature after that the mixture was heated up to 85° C for one hour by magnetic stirrer. The final products were deposited on the glass substrates by chemical spray pyrolysis at 300°C and an atmospheric pressure of 7.5 bar lasting 5 seconds as the Figure1b. The reaction was investigated by the following equation [19]:

$$Na_2S(aq)+ZnCl_2(aq) \longrightarrow ZnS(s) + 2NaCl\,(aq) \quad (1)$$

Table 1. Molarity and weight used of preparation of ZnS thin films.

Concentration (M)	0.1	0.3	0.5
Weight(gm) $ZnCl_2$	0.272	0.544	0.81789
Weight(gm) Na_2S	0.158	0.316	0.474

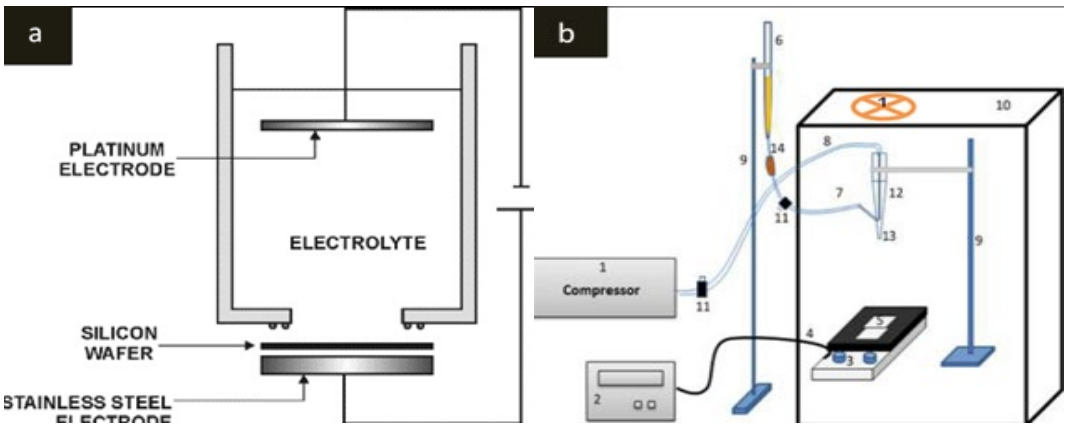

Fig. 1. (a) Set up of Electrochemical cell, (b) Set up of spray pyrolysis.

3. Results and discussion

3.1. Structure properties

XRD patterns of the ZnS nanostructure deposited over glass substrate at concentration 0.1, 0.3 and 0.5M are shown in Figure 2. All the spectra show the peaks related to (111), (002) , (110), (220) and (311) orientations corresponding to zinc blende hexagonal structures ZnS and

corresponding to JCPDS Card No. 00–001–0677 wurtzite ZnS structure with angle (2θ) equal to 31.13°, 27.32° 38.06o 48.31° and 57.81° respectively [15].

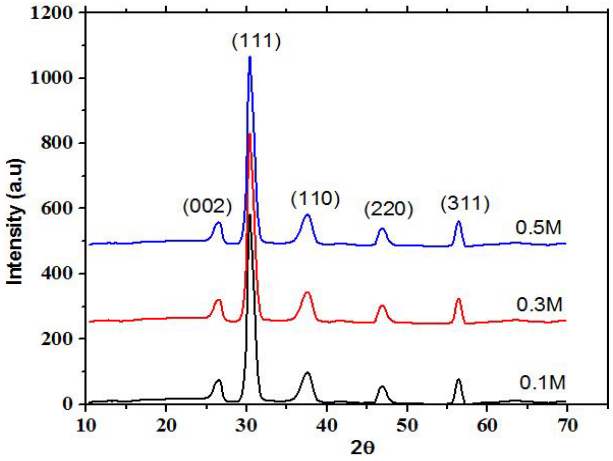

Fig. 2. XRD of ZnS thin films deposited on glass substrate at concentrations (a) 0.1M,(b)0.3M and (c)0.5M.

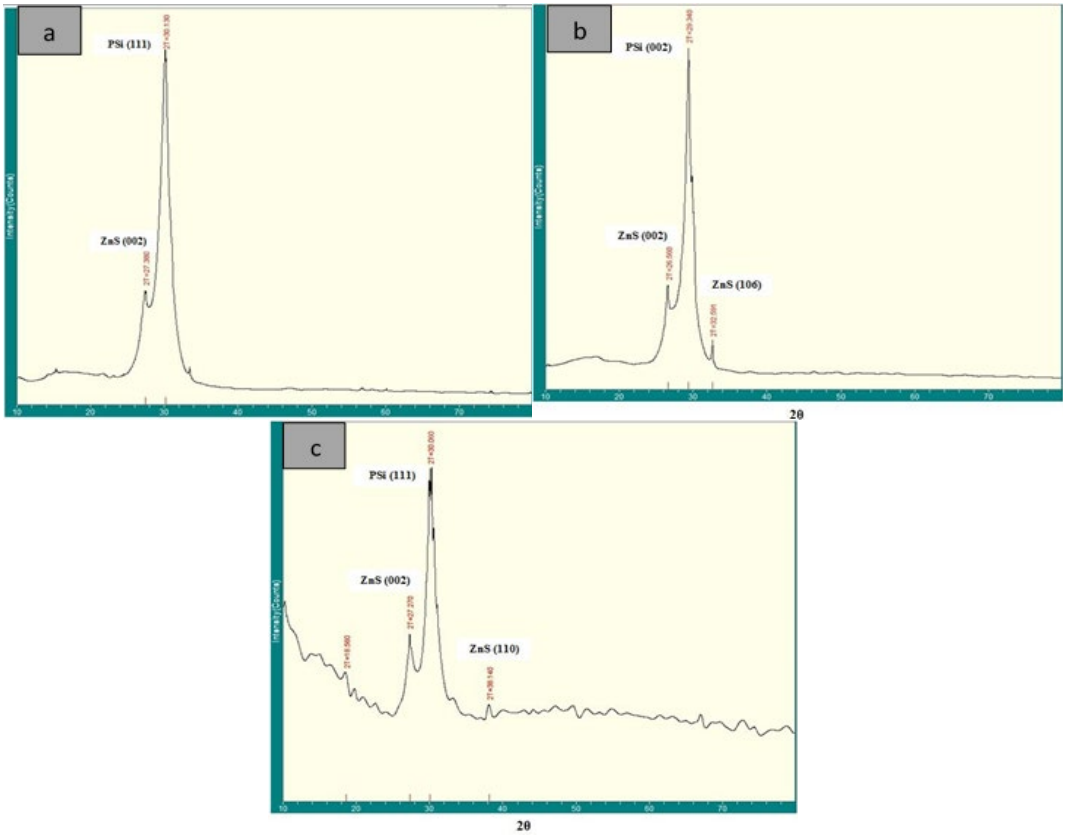

Fig. 3. XRD of ZnS thin films deposited porous silicon at concentrations: (a) 0.1M,(b)0.3M and (c)0.5M

Figure 3(a, b and c) shows the XRD pattern of ZnS/PSi heterojunction when the concentrations of ZnS are 0.1, 0.3 and 0.5 M respectively at etching time of 10 min. It can be seen from Figure 3a that the PSi layer remains crystalline in-plane (111) and (002) with diffraction angle 29.13° and 27.38° respectively which belong to wurtzite ZnS structure. While the films deposited at ZnS concentration of 0.3M showed peaks at (002), (111) and (106) corresponding to

diffraction angle 26.56º, 26.56º and 32.591º respectively as shown in Figure 3b. In addition, the porous silicon peak is shifting slightly to small diffraction angle with increasing concentration. Figure 3c shows the diffraction angle 2θ=30.06º, 27.27º and 38.06º belong to PSi (111), ZnS (002) and ZnS (110) respectively. FWHM of the peaks is directly proportional to the size of the nanocrystalline domain as shown in Table 2. The crystallite size of PS was calculated through the Deby Sherrer formula[20,21].

$$L = \frac{k\lambda}{B\cos\theta} \tag{2}$$

where L is the nanocrystal diameter, λ is the wavelength of light, β is the peak in radian of the full width at half maximum (FWHM), and θ is the angle of Bragg.

Table 2. Crystalline size, FWHM, inter-plane distance (d) of ZnS/Psi.

Sample	Concentration *(M)*	2θ	*hkl*	*L* (nm)	FWHM (deg)	d (Aº)
ZnS/PSi	0.1	27.38	002	37.47	0.561	3.254
		29.13	111	29.561	0.826	3.431
ZnS/PSi	0.3	26.56	002	38.615	0.436	3.174
		29.34	111	30.422	0.723	3.255
		32.591	106	22.633	0.985	3.513
ZnS/PSi	0.5	27.27	002	39.711	0.411	3.251
		29.06	111	33.622	0.633	3.122
		38.06	110	24.799	0.911	3.422

3.2. Scanning electron microscope (SEM)

Figure 4 illustrates SEM images of ZnS/PSi thin films synthesized by spray pyrolysis method at concentration (0.1, 0.3 and 0.5 M). Figure 4 (a and b) show SEM images of PSi at etching time 5 and 15 min. The pore diameter increases with etching time due to dissolution of silicon substrate at the wall of pores. Images also approve sponge-like nanostructures with average diameter 47nm were obtained. Figure 4 (c, and d) shows the SEM image of the ZnS/PSi surface at etching time 5 and 15 min at concentration 0.3M respectively. Results confirm that agglomeration was observed in images with average diameter less than 100 nm were obtained. It seems with concentration ZnS growth stage is preferential compare to nucleation stage. We notice that there is a growth and interference between ZnS nanostructrures with the porous silicon surface, this interference increases with increasing etching time. The deposition of ZnS improves of the structural stability of the porous silicon. These results are agreement with [22].

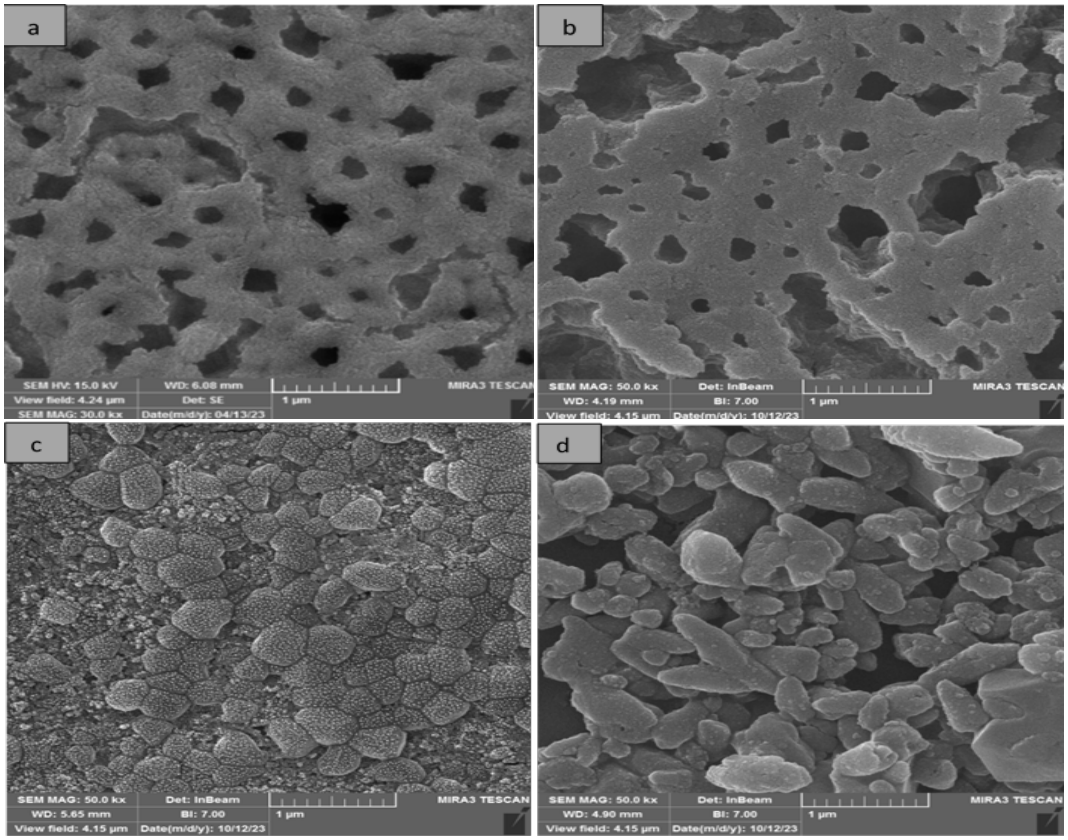

Fig. 4. SEM of ZnS/PSi thin films (a) PSi at etching 5min, (b) PSi at etching 15min and, (c) CuS/PSi of 0.3M at etching time 5 min, (d) CuS/PSi of 0.3M at etching time 15 min.

3.3. Fourier transmission infrared (FTIR)

Figure 5 (a, b and c) shows the typical Fourier transform spectrum (FTIR) of the ZnS nanostructure at concentrations 0.1, 0.3 and 0.5M. The peaks at 482.63, 611.40 cm^{-1} are the characteristic absorption of Zn–S bond. The spectrum indicated strong absorption peaks at 1064.74 cm^{-1} and 3435 cm^{-1}. These are attributed to the stretching modes of C-H group in acetates and –OH group in water respectively and other weak absorption peaks which corresponding to 1629.48 cm^{-1} and 2922.74 cm^{-1} . These are due to the stretching modes of C=O and C-O group respectively as Figure a. Furthermore, the spectrum observed three strong peak at 3434.37 cm^{-1}, 2922.78 cm^{-1} and 1629cm^{-1} due to stretching modes of –OH, C-O and C=O group respectively also presence absorption peak at 821.55 cm^{-1} due to resonance interaction between S^{2-} vibrational mode as Figure b and c. This result show suitable agreement with previous works [23].

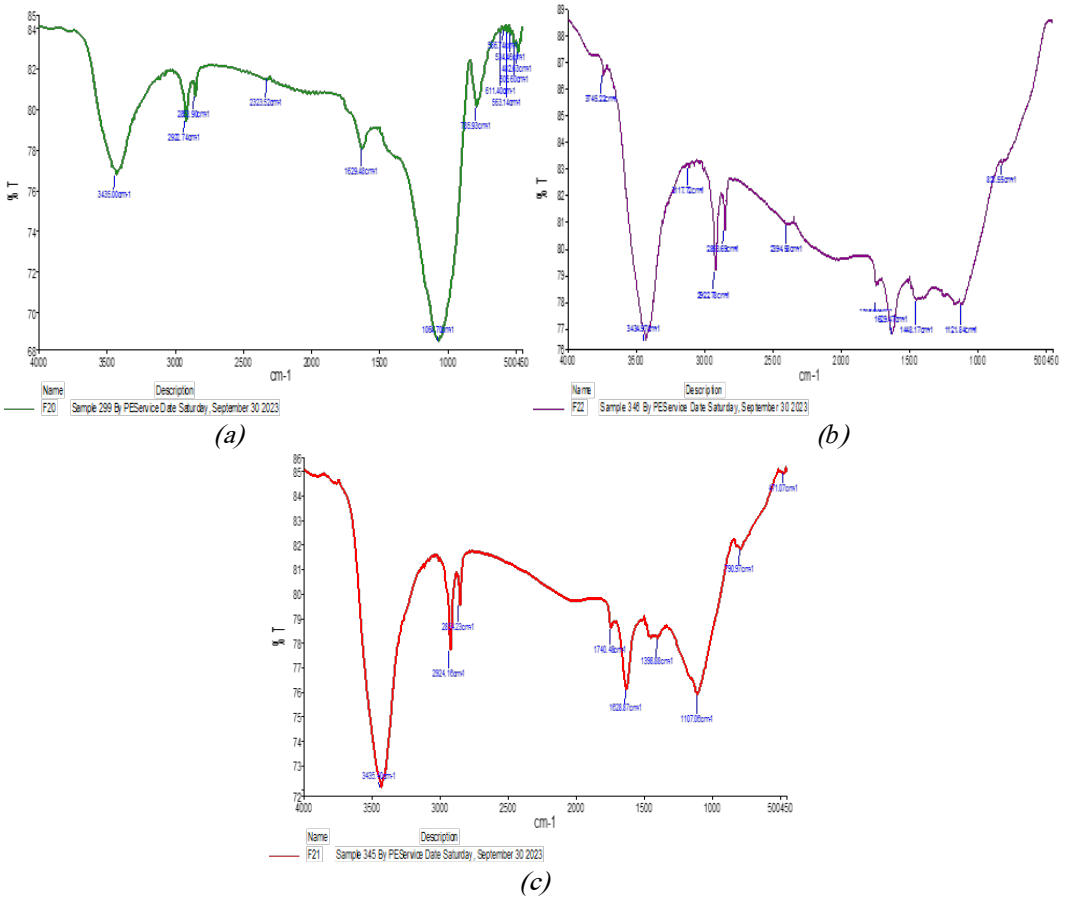

Fig. 5. FTIR of ZnS thin films at concentration (a) 0.1M, (b) 0.3M, (c) 0.5M.

3.4. Optical properties

The optical properties of the ZnS nanostructures were studied by (UV-Spectrophotometer) at different concentration 0.1, 0.3 and 0.5M. Figure 6a illustrates the absorbance peaks as a function of the wavelength. The optical absorption of the film decreases sharply after λ=350 nm. The results show that the absorbance of ZnS thin films were increased with increasing concentration. This may be due to the breaking of bonds on the ZnS surface, which leads to increase the absorbance mechanisms. Increasing of concentration leads to formation defects. These defects are an interested factor in photo electronic devices as they play important role in the optical properties of a material [24].

Fig. 6 b shows the transmittance as a function of the wavelength. The absorbance of ZnS thin films decreased with increasing concentration. The maximum values is found to be 95% at concentration 0.5M. Figure 6c shows the absorption coefficient (α) of ZnS film which is determined from Lambert's law [25]:

$$\alpha = 2.303 \frac{A}{t} \tag{3}$$

where t is the film thickness. We note that the absorption coefficient decreases with increasing wavelength and increases with concentration, as it has high values ($\alpha \geq 10^4$ cm^{-1}) that explain the possibility of direct transitions. The extinction coefficient decreases with wavelength for all samples as Figure 6d. Figure 6(e, f) shows the reflectance spectrum for ZnS thin film. The reflectance (R) has been found by using the relationship [26]:

$$R = 1 - (T + A) \tag{4}$$

where A is the absorbance and T is the transmittance. It is clear that reflectance (R) and refractance (n) decrease with increasing wavelength in the visible region and increase with increasing concentration due to the number of photons that were absorbed in the ZnS thin films.

Fig. 6g shows the relationship between the (α hν)2 and photon energy (hν) of ZnS thin films. This behavior can be justified by generating extra energy states with increasing concentration. Most of defects created by the localization of ions vacancies and change of crystal structure. The energy gap (Eg) may be estimated by Tauc equation [27]:

$$\alpha h\upsilon = B\left(h\upsilon - Eg\right)^{r} \tag{5}$$

where B is constant, α is the absorption coefficient, hυ is photon energy, r takes ½ of direct transition and 2 of indirect transition. The results show, the optical energy gap decreases with number of spray and its values 3.26, 3.21, 3.1 eV for concentration (0.1 ,0.3 and 0.5M) respectively, which in good agreement with reported data for ZnS film deposited by other methods [28].

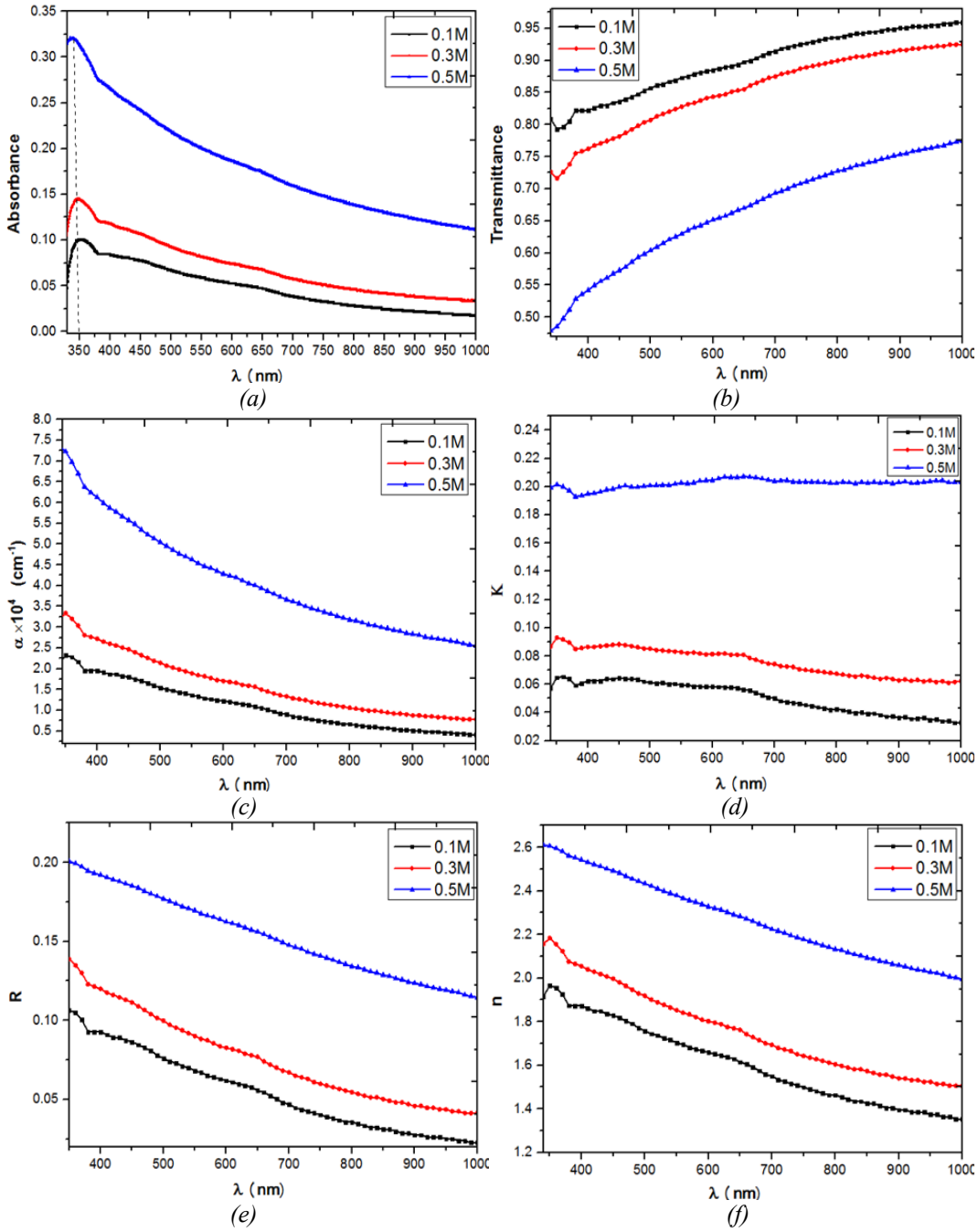

Fig. 6. (a) Absorbance, (b) Reflection, (c) Refractive index ,(d) Extinction coefficient and (e , f) real and imaginary part, (g)Calculation of energy gap of ZnS thin film deposited on glass substrate.

3.5. Gas sensor

Figures 7 and 8 (a-c) show the typical resistance response (kΩ) as a function to the time of gas sensor for different ZnS concentration (0.1 M and 0.5 M). The operating temperature is selected as (RT ^{0}C, 100 ^{0}C and 200 ^{0}C) with fixed NO_2 gas concentration of (75 ppm). The etching time of (5, 10 and 15 min) is selected at ZnS concentration of 0.1 and 0.5M. The results illustrate that the significant variations of resistance for the gas sensor proved the synthesized ZnS over the porous silicon with higher purity and enabling their application in the manufacture of solid-state sensors for NO_2 detection. It is clear from these Figures that the resistance of ZnS /PSi heterojunction increased with increasing temperature. This can be attributed to that the increasing in concentration leads to increase interactivity of surface area with gas molecules[29]. The properties of ZnS/PSi heterojunction as a gas sensing for gases detection are examined. In order to determine the optimum operating temperature, the response of the ZnS /PSi heterojunction based gas sensors to 75 ppm of NO_2 is tested when the operating temperature varied from 50 C^o to 250 C^o. Two concentrations of ZnS thin films of 0.1 M and 0.5 M are precipitated on the PSi. Figure 9 a,b shows the sensitivity of sensor as a function of temperature for ZnS concentration of 0.1 M and 0.5 M respectively when the etching time is varied from 5min to15min with increment step of 5 min. It can be noted that the sensitivity of the sensor is varied with operating temperature. The sensitivity first is increased with increasing the temperature, up to 200 C^o, and then slowly decreased at 250 C^o. In addition, the sensitivity is improved for both concentration of ZnS when the time etching is increased. So, once size pore of PSi is changed, the sensitivity of ZnS /PSi heterojunction is change as well. Furthermore, the sensitivity is increased with increasing the ZnS concentration[30].

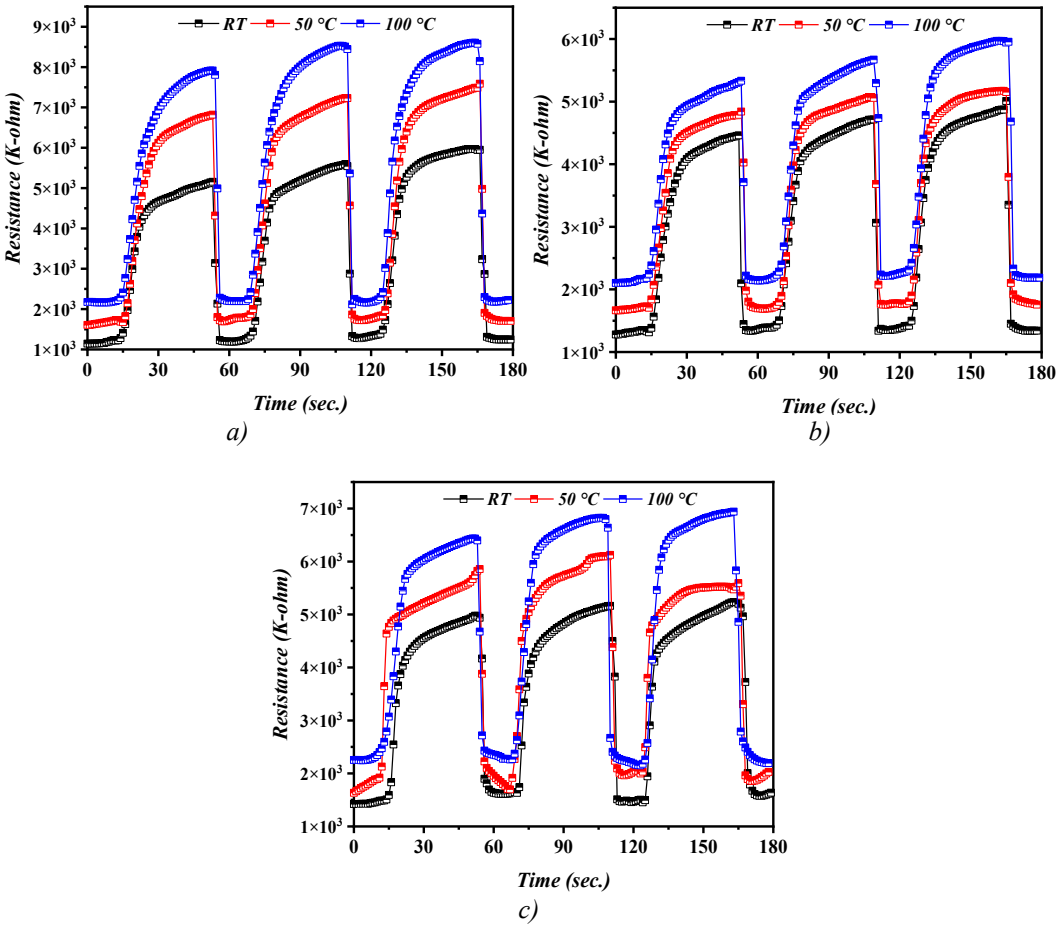

Fig. 7. Switching behavior and Rise/Fall time sensor to 75 ppm of NO_2 gas at (a) RT, (b) 50 °C, (c) 100 °C at etching time 5, 10 and 15 min at concentration 0.1M.

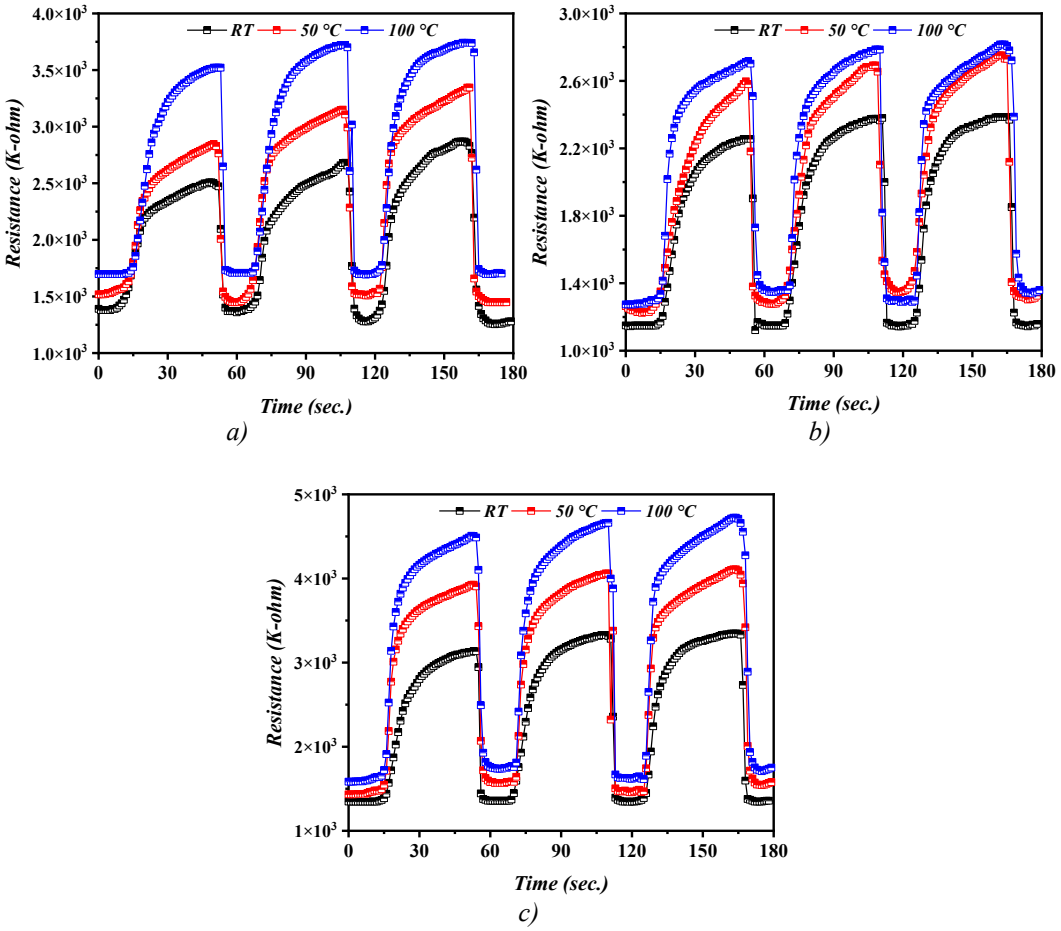

Fig. 8. Switching behavior and Rise/Fall time sensor to 75 ppm of NO_2 gas at (a) RT, (b) 50 °C, (c) 100 °C at etching time 5, 10 and 15 min at concentration 0.5M.

Figure 9 shows the comparison of the sensitivity for ZnS concentration of 0.1 M and 0.5 M when the etching time is 15 min. As can be seen from this Figure, the sensitivity of the ZnS /PSi heterojunction based gas sensor is increased with the increase the ZnS concentration. The maximum sensitivity is found to be 5.11 when the ZnS concentration is 0.5 M compared to the sensitivity of 3.0 at ZnS concentration of 0.1M when the etching time of 15 min. This owing to increase the exposed surface area (increase the walls of the mesoporous structure), at this point, it is important to note that the Schottky barrier created at the ZnS/PSi interface due to the matching of the Fermi level, leading to create a depletion region and interactivity of surface area with gas molecules by the electron adsorption[31]. Tables (3, 4, 5, 6, 7 and 8) show response time, recovery time and sensitivity at different temperatures.

Table 3. Parameter of gas sensor to 75 ppm of NO_2 gas at different temperature at 5min at 0.1M.

	RT	**50 °C**	**100 °C**	**150 °C**	**200°C**	**250°C**
Air	1121.66	1224.047	1231.422	1231.422	1271.422	1251.422
Gas	3035.241	3.40E+03	3.47E+03	3548.241	3735.241	3535.241
G% (NO_2)	1.706026	1.779078	1.814822	1.881418	1.937846	1.82498
Response time (Sec)	4.3	5.8	8.2	11.8	13.51	15.62
Recovery time (Sec)	3.6	3.1	2.9	2.3	2.1	1.9

Table 4. Parameter of gas sensor to 75 ppm of NO_2 gas at different temperature at 10min at 0.1M.

	RT	50 °C	100 °C	150 °C	200°C	250°C
Air	1121.66	1224.047	1241.422	2154.084	1854.848	1322.426
Gas	3135.241	3501.723	3666.233	6941.776	6125.057	4234.195
G% (NO_2)	1.795179	1.860774	1.953254	2.222612	2.302188	2.20184
Response time (Sec)	8.2	9.2	6.5	8.9	9.4	10.2
Recovery time (Sec)	2.1	2.3	2.3	2.4	2.7	2.5

Table 5. Parameter of gas sensor to 75 ppm of NO_2 gas at different temperature at 15min at 0.1M.

	RT	50 °C	100 °C	150 °C	200°C	250°C
Air	1232.676	1665.708	1280.158	1240.158	1260.158	1250.158
Gas	3569.528	5170.168	5009.304	5109.304	5209.304	5009.304
G% (NO_2)	1.895755	2.103886	2.913035	3.11988	3.133849	3.006936
Response time (Sec)	4.2	5.3	4.9	6.8	6.9	7.5
Recovery time (Sec)	2.4	2.3	2.1	1.9	1.8	1.7

Table 6. Parameter of gas sensor to 75 ppm of NO_2 gas at different temperature at 5min at 0.5M.

	RT	50 °C	100 °C	150 °C	200°C	250°C
Air	1232.676	1665.708	1280.158	1240.158	1250.158	1260.158
Gas	3569.528	5170.168	5009.304	5109.304	5309.304	5209.304
G% (NO_2)	1.895755	2.103886	2.913035	3.11988	3.246905	3.133849
Response time (Sec)	6.3	7.8	11.3	13.2	15.4	17.2
Recovery time (Sec)	3.1	2.8	2.3	2.1	1.9	1.8

Table 7. Parameter of gas sensor to 75 ppm of NO_2 gas at different temperature at 10min at 0.5M.

	RT	50 °C	100 °C	150 °C	200°C	250°C
Air	2118.303	1606.957	1250.158	1144.121	1280.158	1380.158
Gas	8604.078	7588.949	6309.304	5969.713	7309.304	7211.304
G% (NO_2)	3.061779	3.722559	4.046804	4.21773	4.709687	4.224983
Response time (Sec)	6.3	7.4	11.5	12.5	13.7	15.2
Recovery time (Sec)	2.8	2.4	2.1	2.2	2.1	1.9

Table 8. Parameter of gas sensor to 75 ppm of NO_2 gas at different temperature at 15min at 0.5M.

	RT	50 °C	100 °C	150 °C	200°C	250°C
Air	1239.158	1244.121	1210.158	1230.158	1260.158	1231.422
Gas	6309.304	6769.713	7309.304	7709.304	8109.304	7535.241
G% (NO_2)	4.091604	4.441363	5.039957	5.26692	5.435147	5.119139
Response time (Sec)	7.8	8.1	8.3	8.6	9.3	9.7
Recovery time (Sec)	2.6	2.3	1.9	1.7	1.6	1.5

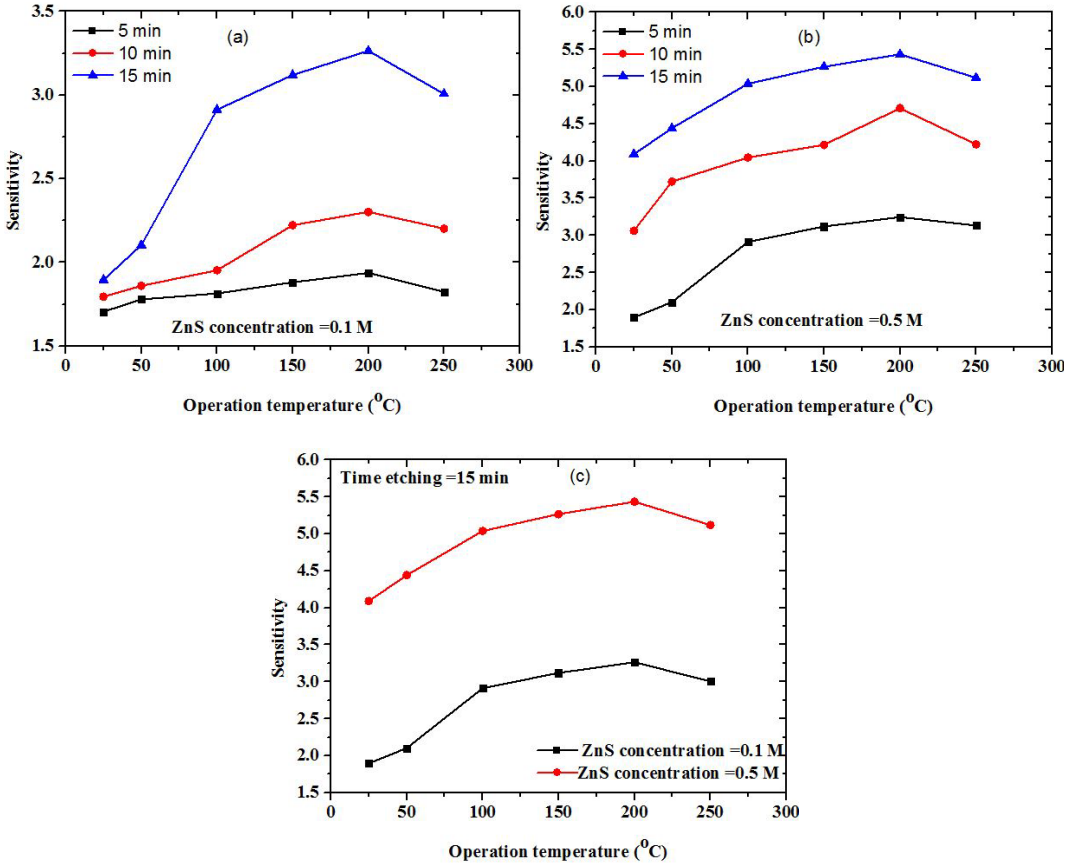

Fig. 9. Sensitivity behavior & operation temperature of NO_2 gas at etching time 5,10 and 15 min at concentration (a) 0.1M , (b) 0.5M , (c) comparison between 0.1 and 0.5M at etching time 15min.

4. Conclusion

In summary, the ZnS/porous silicon hetrostructure as a gas sensor is prepared for sensing NO_2. The spray pyrolysis is a simple and low-cost method which is used to deposit ZnS over the porous silicon substrate. XRD analysis shows that the peaks related to (111), (002), (110), (220) and (311) orientations corresponding to zinc blende hexagonal structures. SEM analysis shows that the pore diameter increases with increasing etching time and approve sponge-like nanostructures with average diameter 47nm. FTIR analysis shows that ZnS/Porous silicon hetrostructure sample presents the peaks at 482.63, 611.40 cm^{-1} ascribed to Zn–S bond. It is found that the prepared ZnS/Porous silicon hetrostructure as sensor is promising for NO_2 sensing. In addition, the sensor has a fast response and recovery times at temperature of 200 °C with fixed NO_2 concentration of (75 ppm). The ZnS may be promising material to amelioration the gas sensor which can be used in different fields such as for UV-light photo-detectors with high sensitivity and fast response.

References

[1] Y. N. Al-Douri, C. Voon, Optik 147, (2017), 343-349; 10.1016/j.ijleo.2017.08.107
[2] Sh. T. Hezarjaribi, N. Shahruz,. J. of Inorganic and Organometallic Polymers and Mater. 30, (2020) 4072-4081; https://doi.org/10.1007/s10904-020-01556-z
[3] O. Bisia, O. Stefano, L. Pavesi, Science Reports 38(12), (2000), 1-126; 10.1016/S0167-5729(99)00012-6

[4] Rehab Joko Hussin, Ivan B. Karomi, Results in Optics 12, (2023) 100452; https://doi.org/10.1016/j.rio.2023.100452
[5] T. Kumeria, J. P. Steven, Sh. M. McInnes, Expert opinion on drug delivery 14(12), (2017) 1407-1422; https://doi.org/10.1080/17425247.2017.1317245.
[6] R. A. Rasool, Ghazwan G. Ali, N. A. Hussein, Digest J. of Nanomaterials and Biostructures 14(3), (2019) 743-750.
[7] A. A. Sulaiman, Ghazwan Gh. Ali, A. Izzalddin Thanon, J. of Nanostructure 12(1), (2022) 1-11.
[8] S. Mohammed, Engineering and Technology Journal 37(1), (2019) 1-4; 10.30684/etj.37.1B.3.
[9] G. G. Ali, M. A. Ahmed, A. A. Sulaiman, Digest Journal of Nanomaterials and Biostructures 17(2), (2022) 473 – 480; 10.15251/DJNB.2022.172.473
[10] H. Föll, M. Christopersen, J. Carstensen, G. A. Hasse, Phys. Stat. Sol. A182 (1), (2000) 7 – 16; 10.1002/1521-396X(200011)182:1<7::AID-PSSA7>3.0.CO;2-B
[11] J. Park, Y. Yanagida, T. Hatsuzawa, Sensors and Actuators B: Chemical 233(11), (2016) 136-143; 10.1016/j.snb.2016.04.058
[12] E. A. Saverina, ACS Sustainable Chemistry and Engineering 8(27), (2020) 10259-10264.
[13]T. A. Aswad, T. A. Abbas, G. G. Ali, Digest J. of Nanomaterials and Biostructures 16(3), (2021) 831–838; 10.15251/DJNB.2021.163.831
[14] J. Andrew, R. James, American Chemical Society 136(44), (2014) 15654–15659; https://doi.org/10.1021/ja5081647
[15] G. G. Ali, A. A. Sulaiman, M. H. Younus, A. M. Mohammed, Res. in Phy. 14, 102466 (2019); https://doi.org/10.1016/j.rinp.2019.102466
[17] C. Wang, Optics & Laser Technology 43(8), (2011) 1453-1457; 10.1016/j.optlastec.2011.04.018
[18] H. P Wang, Z. Zhang, Y. Ning, X. Fang, IEEE Access 7(2), (2018) 19395-19400; 10.1109/ACCESS.2018.2885169
[19] U. M. Nayef, H. T. Hussein, A. M. Abdul Hussien, Optik 172(7), (2018) 1134–1139; 10.1016/j.ijleo.2018.07.112
[20] J. Xu, Int. J. Electrochem. Sci. 14(2), (2019) 5188-5199; 10.20964/2019.06.10
[21] K. Omar, K.A. Salman, Journal of Nano Research 12(2) (2017), 123-134; 10.4028/www.scientific.net/JNanoR.46.45
[22] X. Yang, F. Xi Chen, X. S. Li, S. Li, X. Wan, W. Ma, Fuel Cells 21(1), (2020) 52-57; 10.1002/fuce.202000048
[23] R. Vercauteren, Sensors and Actuators A: Physical 318(12), (2020) 112486; 10.1016/j.sna.2020.112486
[24] M. S. Akhtar, Mater. Chemistry and Phy. 189(3), (2016) 28-34; 10.1016/j.matchemphys.2016.12.027
[25] O. S. Volovlikova, P. Lazarenko, Micromachines 11(2), (2020), 199; 10.3390/mi11020199
[26] D. A. Lizunkova, I. A. Shishkin, N. V. Latukhina, IOP Publishing: Conference Series 1, (2020) 1695; 10.1088/1742-6596/1695/1/012001
[27] Y. Tsai, Vacuum 178(8), (2020) 109454; 10.1016/j.vacuum.2020.109454
[28] M. Mizuhata, M. Yuki, M. Hideshi, Electrochimica Acta 201(3), (2016) 86-95; 10.1016/j.electacta.2016.03.179
[29] A. Kumar, Sensors and Actuators A: Physical 331(5), (2021) 112988; https://doi.org/10.1016/j.sna.2021.112988
[30] M. M. Hassan and M. A. Fakhri, Digest J. of Nanomaterials and Biostructures 14 (4), (2019) 873–878.
[31] I. Sadovnikov, Russian Chemical Reviews 88(6), (2019) 571-582; 10.1070/RCR4867